PERGAMON

Journal of Structural Geology 25 (2003) 1779–1794

JOURNAL OF STRUCTURAL GEOLOGY

www.elsevier.com/locate/jsg

The damage zone-fault core transition in carbonate rocks: implications for fault growth, structure and permeability

Andrea Billi*, Francesco Salvini, Fabrizio Storti

Dipartimento di Scienze Geologiche, Università "Roma Tre", L.go S. L. Murialdo 1, 00146, Rome, Italy

Received 29 May 2002; accepted 6 February 2003

Abstract

We studied the nucleation and growth of cataclastic fault cores from fractured damage zones in extensional and strike-slip fault zones in carbonate rocks. Analysed fault zones have similar protolith lithology and sedimentary fabric, but different geometry, kinematics, size, tectonic environment and deformation history. Orthorhombic rock lithons, a few decimetres in size, characterise the structural fabric of damage zones. Lithons derive from the intersection of a dominant fracture/cleavage set with bedding and/or joints. At the damage zone–fault core transition, orthorhombic lithons reduce in size and approach an isometric shape. Their cross-sectional aspect ratio has an average value of 1.4. Analysed fault cores have similar rock textures, sorting and comminution degree. Particle-size distributions of fault core rocks show linear trends in log-log graphs and average fractal dimension of 2.5. Our results on rock fabrics suggest that fault core development initiates from rock masses in damage zones, where the shape anisotropy of orthorhombic lithons favours additional fracturing at high angle to their long axes. Eventually, smaller, nearly isometric lithons generate from repeated fracturing of orthorhombic lithons. When the aspect ratio of these lithons approaches the threshold value of about 1.4, particle rotation is favoured and cataclastic flow starts. Owing to the granular nature of the damage zone-fault core transitions in carbonate rocks, analogies with the nucleation of deformation bands in sandstones can be established. Our results may be of use to the industry for quantitative characterisation of fault zone permeability. According to the proposed model, radical changes on the permeability properties are expected during the growth of fault cores.
© 2003 Elsevier Ltd. All rights reserved.

Keywords: Fault core; Damage zone; Damage zone-fault core transition; Structural fabric; Rock lithon; Particle-size distribution

1. Introduction

Fault zones commonly consist of a complex array of anastomosed fault surfaces that isolate lenses of fractured and crushed rocks (Davis and Reynolds, 1996). Two structural components characterise fully developed fault zones: a damage zone and a fault core (e.g. Chester et al., 1993; Caine et al., 1996). Fault cores and damage zones show different permeability properties relating to different deformational features (e.g. Evans, 1990; Antonellini and Aydin, 1994, 1995; Evans et al., 1997; Knipe, 1997; Manzocchi et al., 1999; Yielding et al., 1999). Fault cores consist of low permeability cataclastic rocks where slip is localised and pre-existing, sedimentary and tectonic structures are fully obliterated by cataclastic flow (e.g. Sibson, 1977). Damage zones consist of rock volumes affected by fault-related fracturing. In damage zones, bedding surfaces and inherited structural fabrics are commonly preserved.

Numerous field and laboratory studies have been carried out on the evolution of fault cores (e.g. Engelder, 1974; Mandl et al., 1977; Aydin, 1978; Aydin and Johnson, 1978; Newman and Mitra, 1993; Marone, 1995; Billi et al., 2003; Storti et al., 2003) and damage zones (e.g. Evans and Langrock, 1994; McGrath and Davison, 1995; Schulz and Evans, 1998, 2000; Davis, 1999; Hesthammer et al., 2000), whereas the transition in space and time from damage zones to fault cores is less well investigated (Hadizadeh and Rutter, 1983). This, in particular, applies to carbonate rocks.

We describe, in quantitative terms, structural fabrics developed in fault zones from shallow-water carbonate rocks in the Southern Apennines, Italy (Fig. 1). In particular, we focus on the structural fabric developed at damage zone–fault core (DZ–FC) transitions in order to define the critical structural texture of rocks controlling the fault core nucleation. Similar results obtained from different fault

* Corresponding author. Tel.: +39-065-4888016; fax: +39-065-4888201.

E-mail address: billi@uniroma3.it (A. Billi).

0191-8141/03/$ - see front matter © 2003 Elsevier Ltd. All rights reserved.
doi:10.1016/S0191-8141(03)00037-3

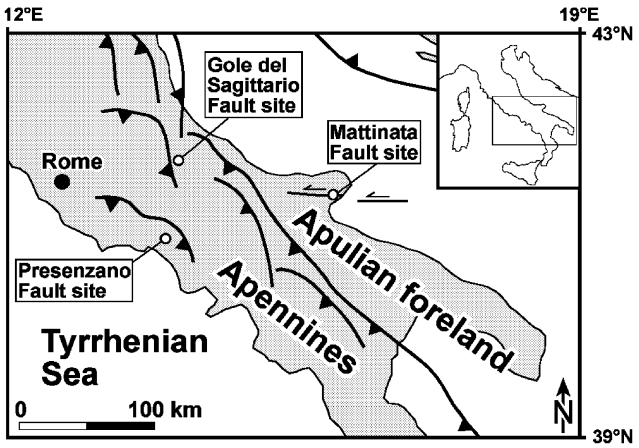

Fig. 1. Location map of fault sites.

zones allow us to propose a genetic model for fault core nucleation and development in carbonate rocks.

2. Methodology

We investigated fault zones by measuring structural elements and sampling cataclastic rocks along outcrop scan-lines. In describing the structural fabric of damage zones, we use the term fracture to include all brittle deformational features, i.e. joints, small-scale faults and solution cleavages (e.g. Pollard and Aydin, 1988). With the term foliation we comprehend bedding and fractures (Davis and Reynolds, 1996).

Analysed fault zones are typically organised as in Fig. 2, with a damage zone encompassing the fault core. The fault core is bounded on one side by the master fault surface. On the other side, the damage zone gradually fades into the fault

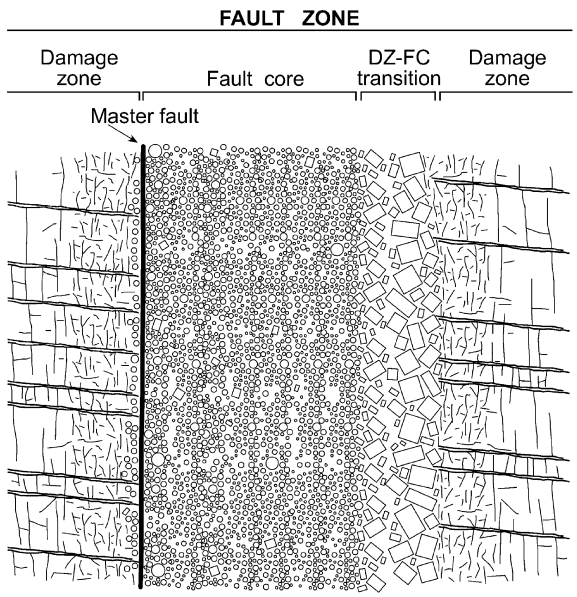

Fig. 2. Conceptual sketch of a fault zone sectioned perpendicular to the shear direction (not to scale).

core. In the field, we differentiated damage zones from fault cores on the basis of the occurrence of cataclastic rocks that are typical of fault cores.

In damage zones, we measured attitude, spacing and crosscutting relationships of foliations. In DZ–FC transitions, we measured the size of rock lithons generated by the intersection of fracture sets. Fracture intersection occurs at angles in the 90° ± 15° range such that resulting lithons are nearly orthorhombic (i.e. three mutually perpendicular symmetry axes, all of different lengths). Photographic slides of rock exposures projected at the 2:1 scale provided detailed sections for size measurements of rock lithons. We acquired slides such that the camera point of view was parallel to the strike of the dominant fracture set (i.e. against which other fracture sets abut). From direct tracing on 2:1 scale slide projections, we computed the two-dimensional aspect ratio (A_r) of one hundred sections (i.e. the lithon face normal to the strike of the dominant fracture set) of rock lithons for each scan-line, where A_r is the ratio of the longer (L) to the shorter (l) sides of the rectangle best circumscribing the section of each lithon. The quasi-rectangular shape of rock lithon sections justifies this approximation. We computed the mean aspect ratio (mA_r) by best fitting the A_r population of each scan-line with an unimodal Gaussian curve (e.g. Salvini et al., 1999). In order to obtain a value of mA_r representative of each DZ–FC transition, the measured lithon sections were randomly chosen over the entire exposure of each analysed DZ–FC transition. We did not assess possible gradients of A_r along DZ–FC transitions.

In fault cores, we analysed the particle-size distributions of bulk cataclastic rocks and computed their fractal dimensions (D) in order to obtain insights into the fragmentation modes and comminution degree. Several studies, in fact, demonstrated that: (1) fractal distribution is the best way for describing particle-size populations of fault rocks (e.g. Sammis et al., 1986, 1987; Marone and Scholz, 1989; Sammis and Biegel, 1989; Blenkinsop, 1991); (2) D values differ with fragmentation modes (Allègre et al., 1982; Turcotte, 1986; Sammis et al., 1987; Blenkinsop, 1991). We performed particle-size analyses through a sieving and weighting technique (Sammis et al., 1986), by using a seven-sieve array (i.e. mesh net aperture from 4.00×10^{-3} to 0.63×10^{-4} m) for dry sieving, and a high precision balance for weighting the residual fraction in each sieve. We computed the number of equivalent spherical particles of each fraction through the reference spherical volume of the corresponding mesh aperture. The resulting equivalent particle populations have a power-law size distribution, as indicated by the linear best fit of data on log-log graphs, in which particle-size (S) is plotted versus particle-size rank (N) (e.g. Turcotte, 1986; Cladouhos and Marrett, 1996). The fractal relationship of particle frequency by size is

$$N_S \approx S^D \quad (1)$$

where N_S is the number of equivalent particles of size $\leq S$,

and D (i.e. fractal dimension) is the slope of the best fit line (e.g. Blenkinsop, 1991).

3. Fault zone analysis

3.1. Strike-slip faulting through slightly deformed protolith

We investigated the structural architecture of strike-slip faulting through slightly deformed carbonate protolith on exposures of the Mattinata Fault (S. Simeone Quarries in Fig. 3). The Mattinata Fault is an E–W-trending, left-lateral, strike-slip fault zone exposed for more than 40 km in the Apennines foreland, Southern Italy (Billi and Salvini, 2000, 2001). The fault zone is well exposed and reaches 200–300 m in width. Thick bands of cataclastic rocks and severely damaged carbonate rocks are exposed at S. Simeone Quarries, located within a slightly transpressional segment of the Mattinata Fault. The protolith is a slightly deformed shallow-water limestone of Jurassic age. Limestone beds strike E–W and dip southwards by about 20°. At S. Simeone Quarries, we carried out four scan-lines across the DZ–FC transition of the Mattinata Fault (Fig. 4). In the studied scan-lines, master faults are strike-slip

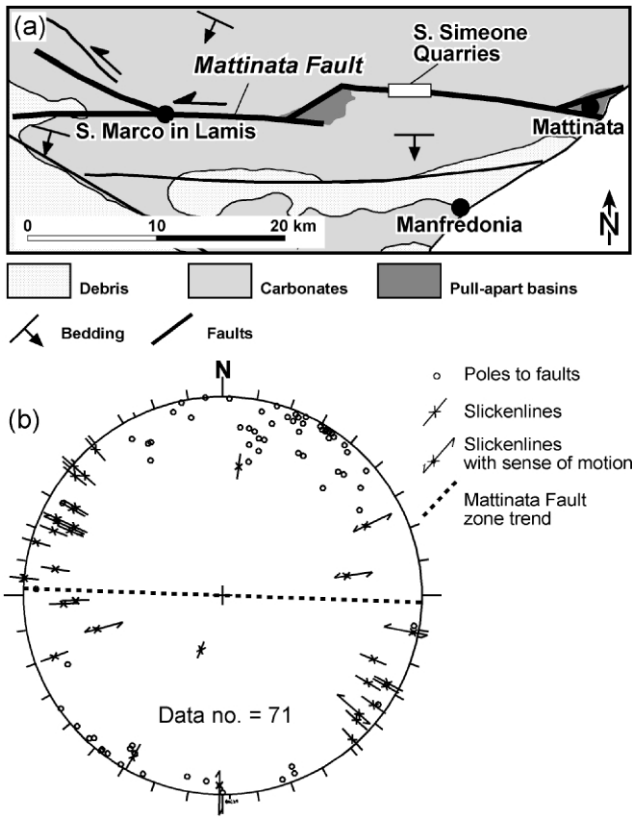

Fig. 3. (a) Structural sketch of the Mattinata Fault area (southern Gargano Promontory) and location map for S. Simeone Quarries. (b) Stereograms (Schmidt projections, lower hemisphere) representing fault poles and slickenlines sampled at S. Simeone Quarries. Dashed line is the trend of the Mattinata Fault zone at the S. Simeone Quarries.

surfaces striking between N60° and N150°. The dominant fracture set in the damage zone consists of NW-striking, sub-vertical solution surfaces with a spacing of a few centimetres (0.1–7.0 cm; Fig. 5a). Sub-horizontal and sub-vertical joints abut against cleavage surfaces (Fig. 4a and b). Both solution structures and joints are genetically related to the fault activity and development of solution surfaces predated jointing (Salvini et al., 1999). The resulting three-dimensional fracture network defines a pattern of unrotated, nearly orthorhombic lithons with the short symmetry axis perpendicular to the cleavage surfaces. The thickness of the DZ–FC transition varies between 1 and 2 m. There, rock lithons reduce to a few centimetres (1–5 cm) in size by the increase of joint frequency, and tend towards a tetragonal (i.e. three mutually perpendicular symmetry axes, two of equal lengths) or isometric (i.e. three mutually perpendicular symmetry axes, all of equal lengths) shape by reducing the length of long axes and preserving the short (i.e. perpendicular to cleavage) axis. Pressure-solution mechanisms may have also promoted a reduction of lithon size, that is negligible or slightly significant when compared with that generated by multiple fracturing. In this fault region, several lithons show crushed edges and evidence of slight rotations. The geometrical analysis of rock lithon sections in the DZ–FC transition gives mA_r values of 1.4 (MAT-1, -3 and -4) and 1.3 (MAT-2) with a standard deviation (sd) of 0.5 (Fig. 6). Fig. 7 shows that the short side, l, of rock lithon sections (mean value = 10.5 mm, sd = 6.2) approximately coincides with the cleavage spacing (mean value = 10.8 mm, sd = 7.0).

In the fault core, the rock fabric changes from fracture-dominated to cataclastic (Fig. 5c). Cataclastic rocks are of poorly indurated cataclasites with a few survivor grains entirely surrounded by a finer matrix. The absence of pre-existing sedimentary/tectonic structures (Fig. 5c) document particle rotation and translation in fault cores (i.e. cataclastic flow). Particle-size distributions of cataclastic rock samples in log-log graphs (Fig. 8) have fractal dimensions that vary between a minimum of 2.15 (sample 4GA5) and a maximum of 2.77 (sample 3GA4).

3.2. Extensional oblique-slip faulting through deformed protolith

We investigated the structural architecture of extensional oblique-slip faulting through deformed protolith on a road-cut exposure across the Presenzano Fault. The Presenzano Fault is a NNE-striking, WNW-dipping, oblique extensional (i.e. right-lateral), outcrop-scale fault zone. The fault surface is exposed in Early Jurassic carbonate rocks for approximately 0.7 m along-strike and 3 m across strike. The Mesozoic carbonate succession in this region is affected by contractional and strike-slip deformations, overprinted by younger extension along NE- and NW-trending faults, which are Pleistocene to Recent in age (Parotto, 1971; Parotto and Praturlon, 1975; Bosi and Giordano, 1997). The

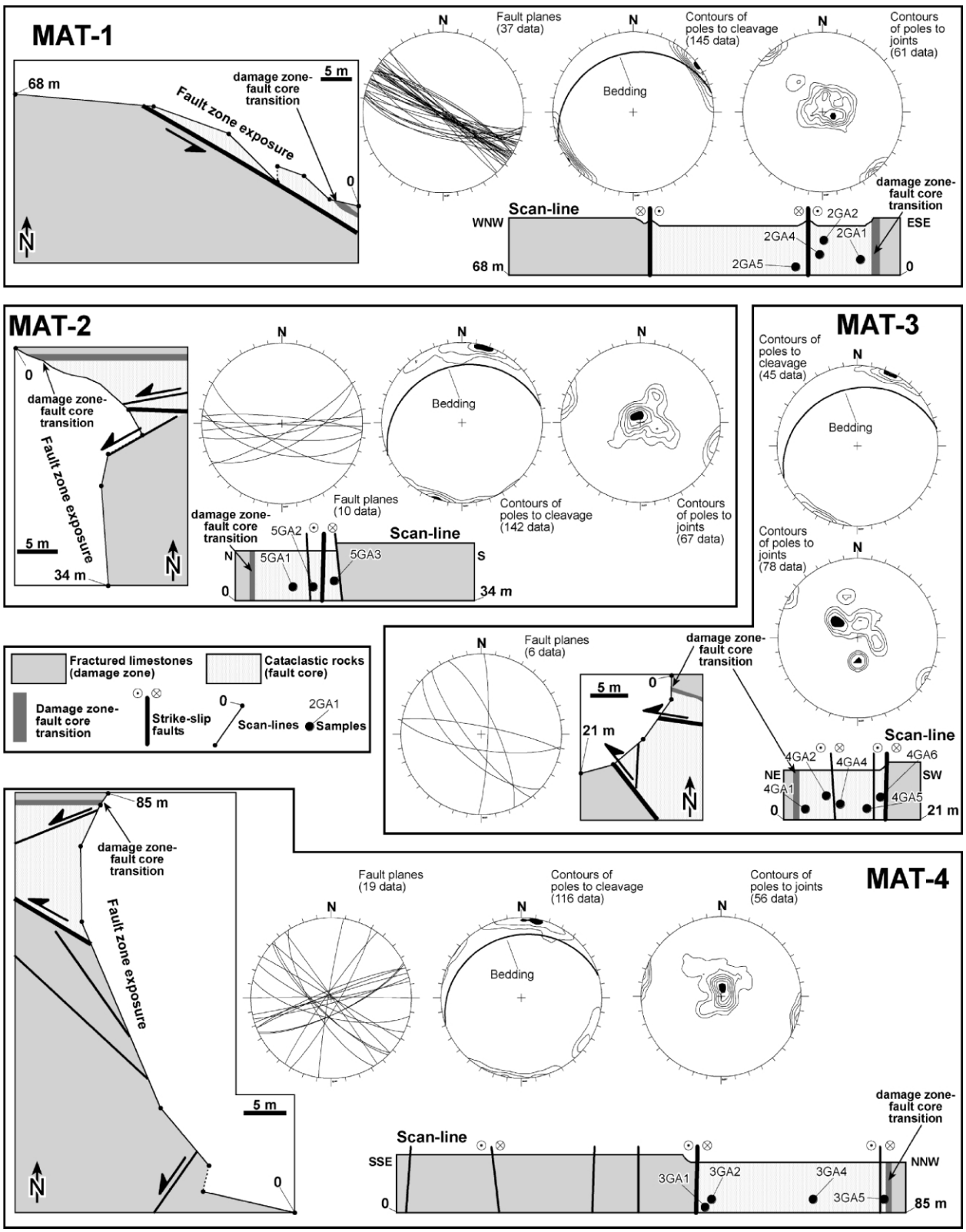

Fig. 4. Map views, schematic cross-sections and stereograms (Schmidt projections, lower hemisphere) of structural data, for MAT-1, MAT-2, MAT-3 and MAT-4 scan-lines (Mattinata Fault zone).

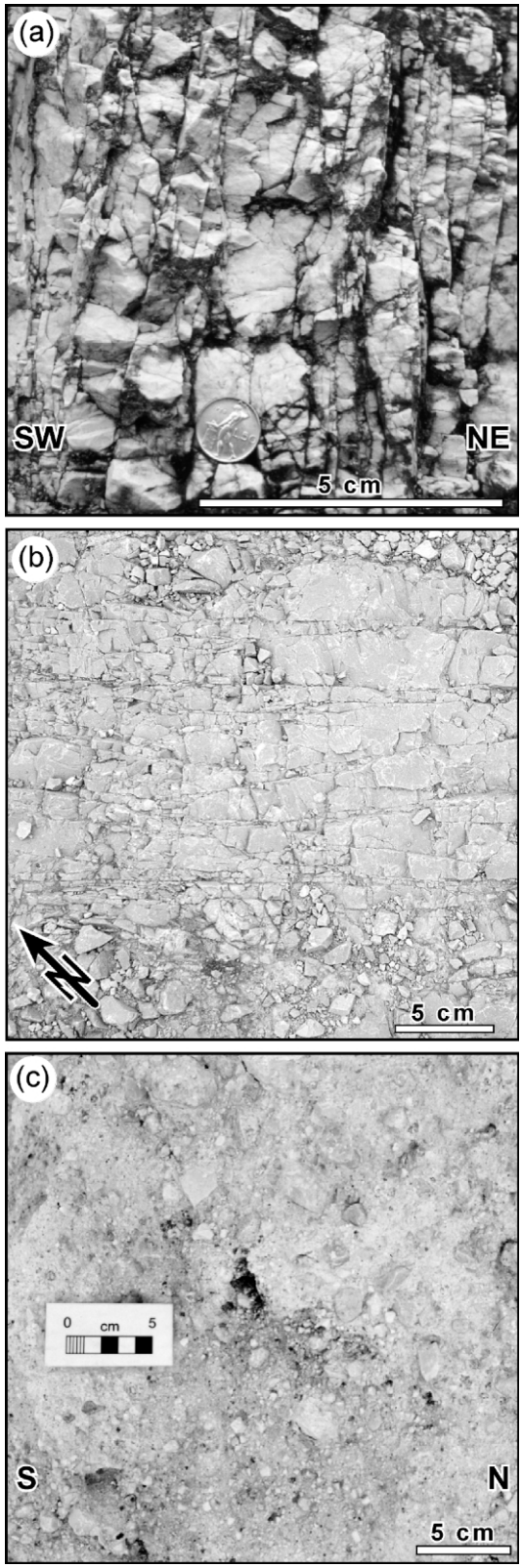

Fig. 5. Outcrop photographs showing fault-related rocks at the S. Simeone Quarries (Mattinata Fault zone). (a) Vertical, cross-sectional views of dominant cleavage domains in the damage zone. Sub-horizontal transverse joints abut against cleavage surfaces forming a pattern of juxtaposed, interlocked lithons. (b) Map view (perpendicular to (a)) of cleavage domains dissected by sub-vertical transverse joints. (c) Vertical cross-sectional view of fault core rocks.

fault zone consists of a fault core occurring in the hanging wall (Fig. 9a). The thickness of the damage zone in the footwall is approximately 0.5–1.0 m. The remaining portion of the footwall is a carbonate protolith with inherited fractures. This fracture pattern consists of small faults and solution cleavages (Fig. 9a). Faults are high-angle, oblique- to strike-slip surfaces striking N80° and N150–160°, respectively. Cleavages consist of closely spaced, subvertical solution surfaces that preferentially strike N160°. In the damage zone, two sets of sub-horizontal and sub-vertical joints dissect the solution cleavage domains (diagrams in Fig. 9a and photograph in Fig. 9b). Joints perpendicularly abut against cleavage surfaces. Cleavage formation predated jointing. The intersection of joints and solution cleavages defines nearly orthorhombic rock lithons. In the DZ–FC transition (hanging wall side in Fig. 9a), rock lithons change from orthorhombic to nearly isometric. Their long axis is 4–5 cm at maximum, and mA_r is 1.4 with a standard deviation of 0.5 (Fig. 9b).

The fault core abuts against the N17°-striking, WNW44°-dipping master fault on the east side (i.e. footwall side in scan-line of Fig. 9a), and grades a few centimetres (10–20 cm) upward into the damage zone on the west side (i.e. hanging wall side). The fault surface is made up of indurated cataclasites. The fractal dimension D from particle-size distributions of cataclastic rocks is 2.48 for the 1PR1 sample and 2.57 for the 1PR3 sample, respectively (Fig. 9c).

3.3. Extensional faulting through strongly deformed protolith

We investigated the structural architecture of extensional faulting through strongly deformed protolith in the Gole del Sagittario Fault, Central Apennines (Fig. 1). The Gole del Sagittario Fault is a NW-striking, SW-dipping extensional fault zone approximately 2×10^3 m long (Fig. 10a). The fault is exposed in shallow-water limestone of Mesozoic age, in the hanging wall of a NE-verging, Pliocene thrust system (Miccadei, 1993). The thrust system is dissected by a NNW–SSE left-lateral, strike-slip to transpressional fault zone paralleling the thrust ramp zone. The Gole del Sagittario Fault developed within this strike-slip brittle shear zone. The master slip surface is fully exposed for approximately 50 m along-strike, and up to 25 m across-strike in the Cava di Rena quarry, where a scan-line (GoS-1) was carried out for a total length of 54 m from the footwall to the hanging wall across the damage zone and the fault core (Fig. 10b). Damage zone and fault core develop in the hanging wall of the Gole del Sagittario Fault (Fig. 9b and c). The master fault surface bounds the fault core on one side (Fig. 10c). On the other side, the fault core grades upward into the damage zone. The footwall shows no extension-related damage, but preserves a well-developed fracture pattern inherited from previous thrust and strike-slip faulting. This fracture pattern consists of

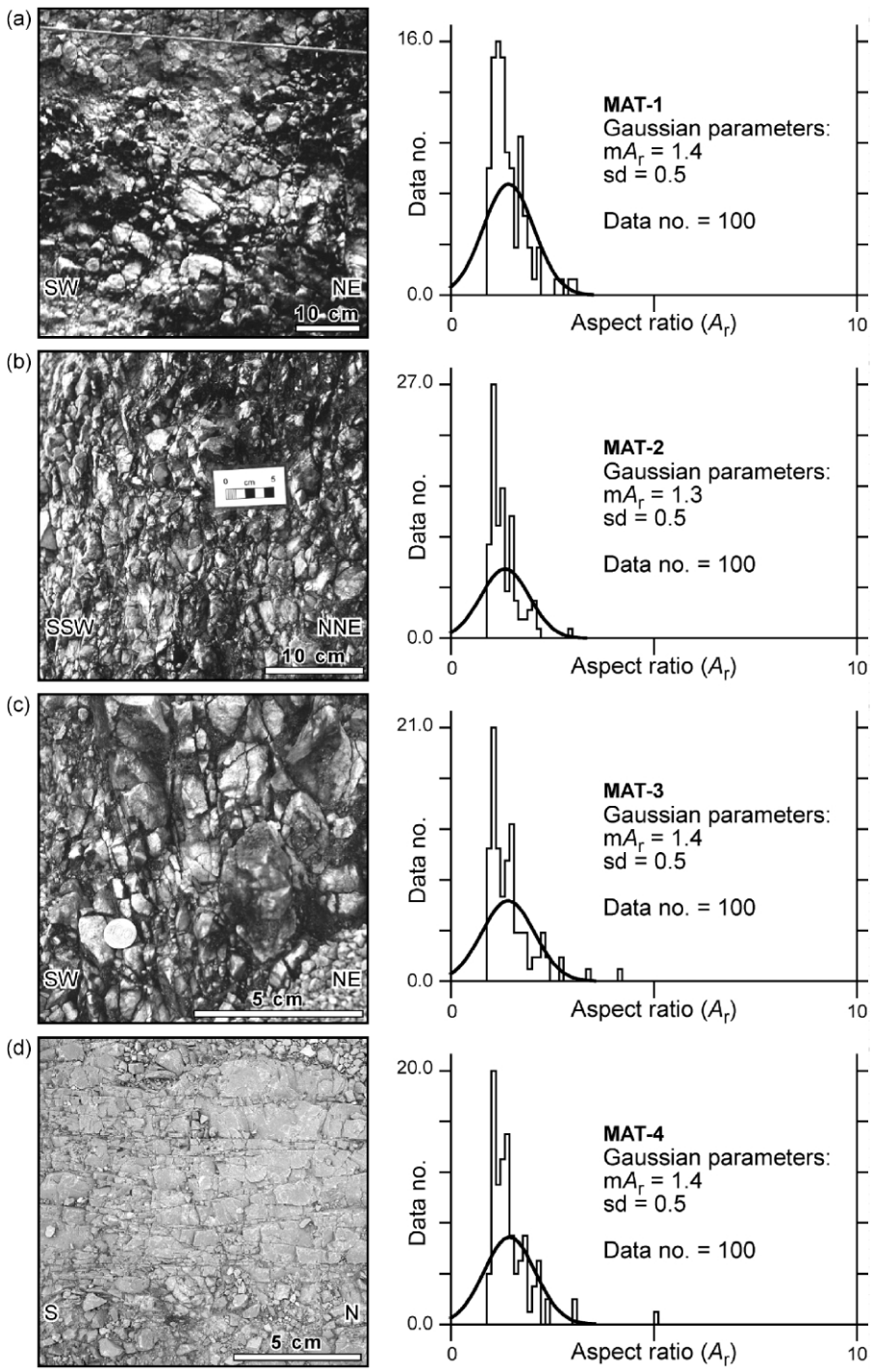

Fig. 6. Outcrop photographs and histograms of A_r (L/l, aspect ratio of lithon sections) at DZ–FC transition for (a) MAT-1, (b) MAT-2, (c) MAT-3, and (d) MAT-4 scan-lines (see locations in Fig. 4). Solid line in histograms is the Gaussian curve best fitting A_r population.

(1) N-striking subvertical solution cleavages, (2) NE-striking subvertical joints, and (3) NW-striking, SW-dipping joints (Fig. 10d). The fracture pattern in the damage zone (i.e. hanging wall side in Fig. 10c) consists of three main sets: (1) N-striking solution cleavages, (2) N50°-striking joints, and (3) N140–150°-striking joints and faults with both NE and SW dips (Fig. 10d). The first two sets are parallel to fracture sets in the footwall. The first set is the dominant fracture family in the damage zone. Fracture spacing in the damage zone is in the order of a few centimetres (2–4 cm). The resulting fracture network in the damage zone generates a rock fabric (Fig. 11a) consisting of triclinic (i.e. three symmetry axes, all of them are unequal in length, none of them are right angles to each other) to orthorhombic lithons a few centimetres in size (4–10 cm). In the DZ–

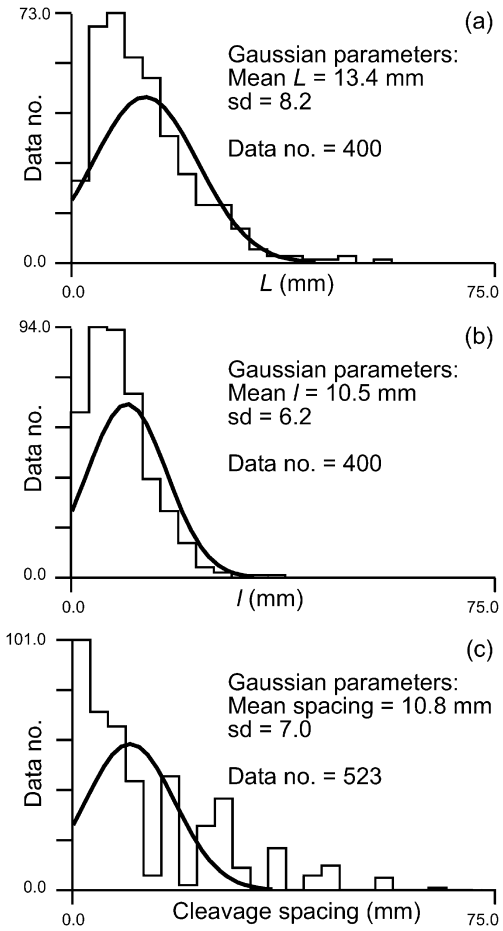

Fig. 7. (a) Histogram of L (long side of lithon sections) population as sampled at damage zone-fault core transition within the Mattinata Fault zone. Solid line is the Gaussian curve best fitting L population. (b) Histogram of l (short side of lithon sections) population as sampled at damage zone-fault core transition within the Mattinata Fault zone. Solid line is the Gaussian curve best fitting l population. (c) Histogram of cleavage spacing as sampled within the Mattinata Fault zone. Solid line is the Gaussian curve best fitting cleavage spacing population.

FC transition (i.e. hanging wall side in Fig. 10c), lithons reduce in size (2–4 cm) and approach an isometric symmetry. A_r measured at the DZ–FC transition has a mean value (mA_r) of 1.4 with a standard deviation (sd) of 0.5 (Fig. 11a).

The fault core develops on the hanging wall side and is approximately 2 m thick (Fig. 10c). The fault core consists of fine-grained, loose cataclastic rocks with a fractal dimension D of 2.24 for the SA3 sample and 2.60 for the SA5 sample (Fig. 11b).

3.4. Structural summary

The analysed fault zones differ by kinematics, geometry, size, tectonic environment and deformation history of protoliths (Table 1). Damage zones differ by structural architecture of fracture arrays. Despite these differences, striking similarities characterise the investigated DZ–FC transitions and fault cores: (1) in DZ–FC

Table 1
Summary of structural data collected from the investigated fault zones

	Strike-slip faulting	Extensional oblique-slip faulting	Extensional faulting
Fault name	Mattinata Fault	Presenzano Fault	Gole del Sagittario Fault
Lithology	Shallow-water layered limestone	Shallow-water layered limestone	Shallow-water layered limestone
Bed thickness	0.5–1.5 m	0.5–1.5 m	0.2–1.0 m
Rock age	Jurassic	Jurassic	Jurassic
Tectonic environment	Foreland	Thrust belt	Thrust belt
Fault zone thickness	~200 m	~3 m	~45 m
Protolith inherited fabric	Widely spaced joints (mostly undeformed)	Strike-slip solution cleavage (deformed)	Joints + faults + solution cleavage (strongly deformed)
Damage zone fabric	Joints + faults + solution cleavage (orthorhombic lithons)	Joints + faults + solution cleavage (orthorhombic lithons)	Joints + faults + solution cleavage (triclinic to orthorhombic lithons)
Damage zone-fault core transition fabric	Joints + faults + solution cleavage (nearly isometric lithons)	Joints + faults + solution cleavage (nearly isometric lithons)	Joints + faults + solution cleavage (nearly isometric lithons)
fault core fabric	Cataclastic	Cataclastic	Cataclastic
Damage zone/fault core relations	Fault core within damage zone	Fault core within damage zone	Fault core at one edge of damage zone
Fault core/master slip surface relations	Master slip surface at one edge of fault core	Master slip surface at one edge of fault core	Master slip surface at one edge of fault core
mA_r	1.3 and 1.4	1.4	1.4
D	2.15–2.77	2.48 and 2.57	2.24 and 2.60

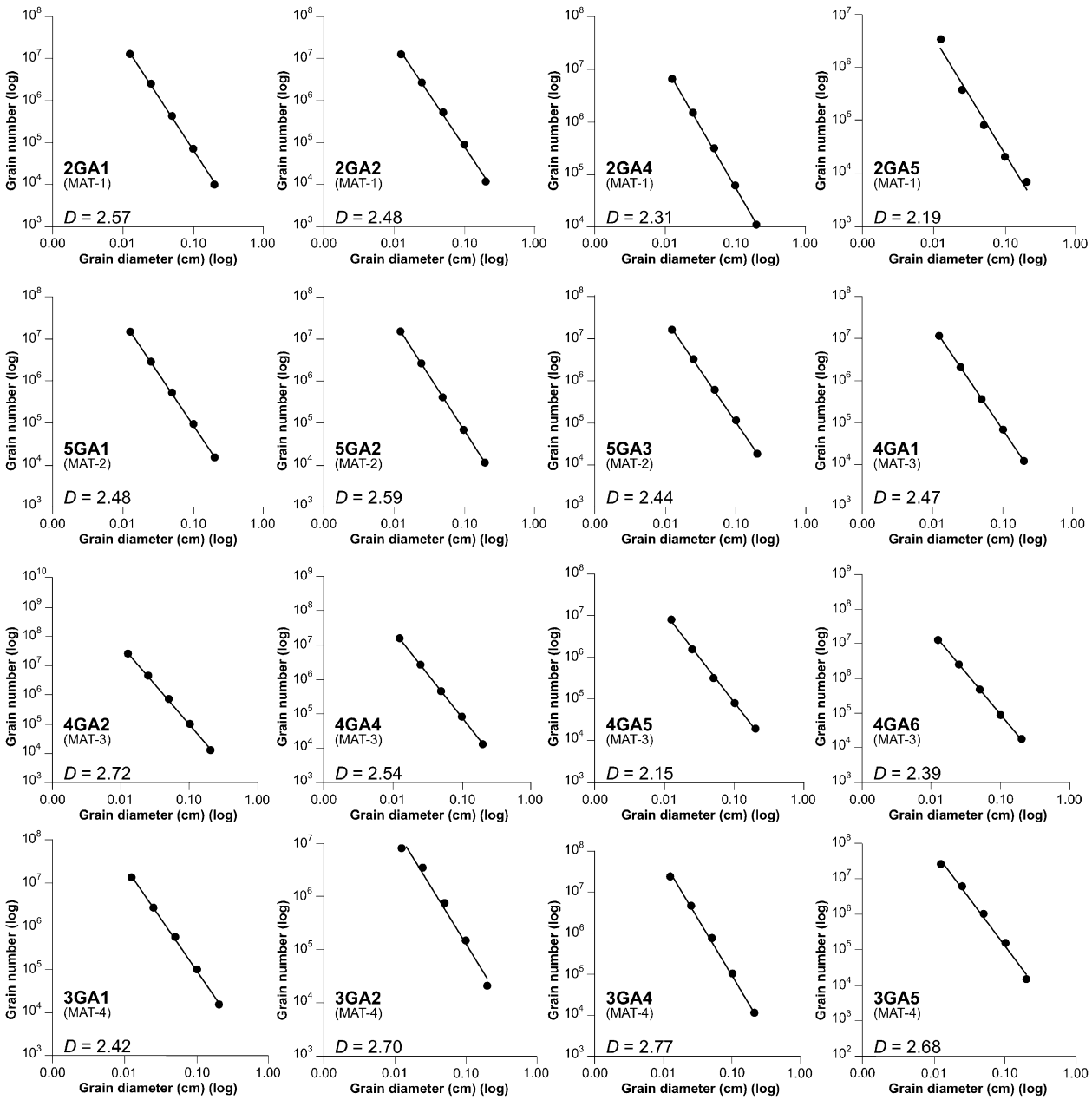

Fig. 8. Log-log diagrams for grain size distribution (grain number vs. grain diameter) of cataclastic rock samples from the Mattinata fault core. Sample location along scan-lines is in Fig. 4.

transitions, at least three fracture sets occur, intersecting at high angle. One of them is the dominant fracture set, which is pervasive in the whole damage zone. The other sets abut against the dominant fracture set. (2) The intersection of fracture sets in the DZ–FC transition produces a structural fabric consisting of nearly isometric lithons of centimetric size. Lithons show an average cross-sectional aspect ratio, A_r, of 1.4 (sd = 0.5; Fig. 12a), which is independent from the lithon dimensions (Fig. 12b). (3) Rocks in fault cores have similar cataclastic fabrics and their particle-size distributions obey a power-law with an average fractal dimension of 2.50 (sd = 0.16; Fig. 12c).

4. Discussion

4.1. Evolutionary model

We interpret the DZ–FC transitions observed in the studied fault zones as the relic structures of embryonic fault cores. Their similar fabrics in fault zones that are different by kinematics and size support the occurrence of a critical rock texture before fault core development can initiate, regardless of any specific attribute of the fault zones. Based on this assumption and on the above-summarised structural observations, we propose a general evolutionary model of fault core development from damage zones in carbonate

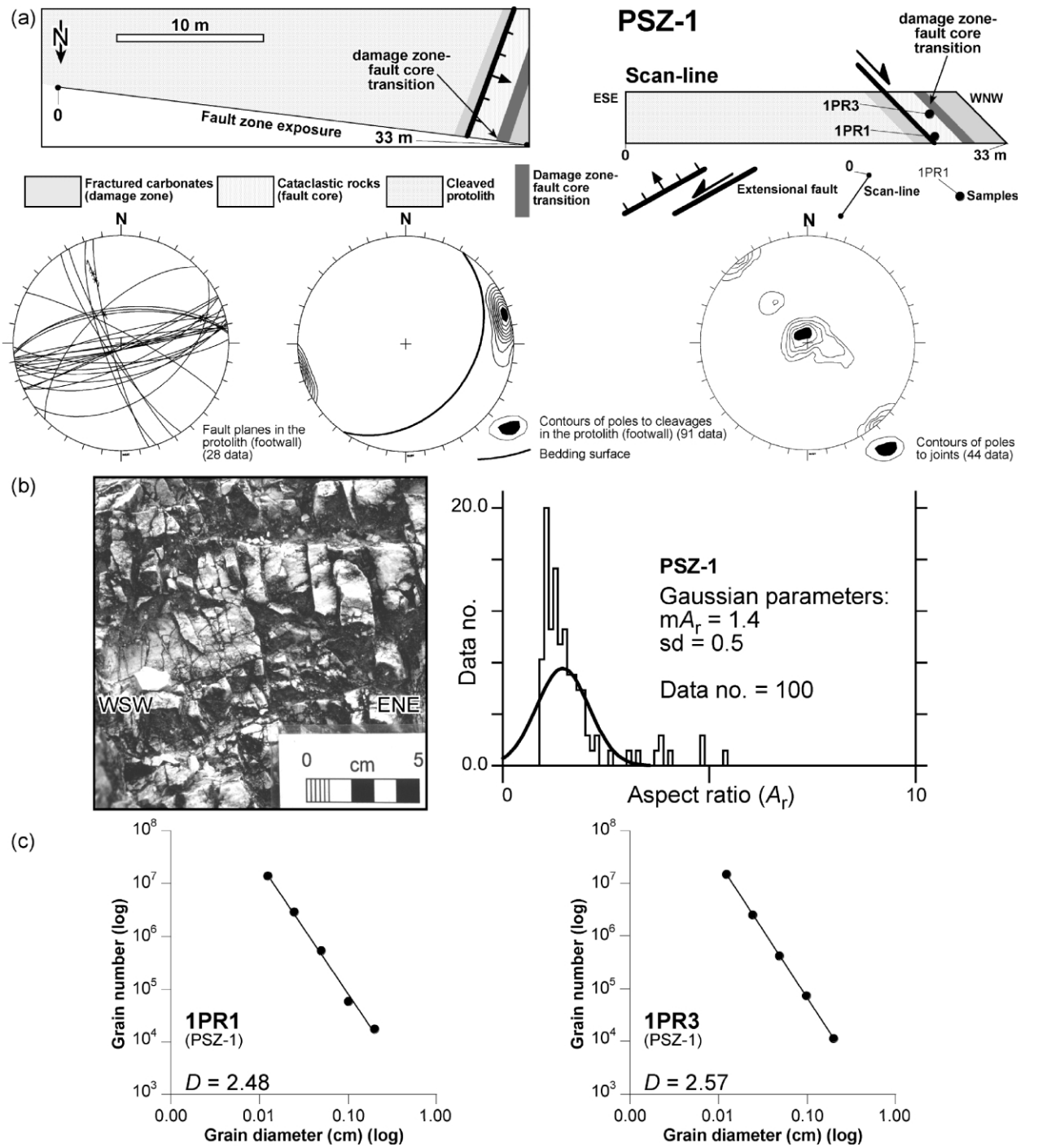

Fig. 9. (a) Map view, schematic cross-section and stereograms (Schmidt projections, lower hemisphere) of structural data for PSZ-1 scan-line (Presenzano Fault zone). (b) Outcrop photograph and histogram of A_r (L/l, aspect ratio of lithon sections) at DZ–FC transition for PSZ-1 scan-line. Solid line in histogram is the Gaussian curve best fitting A_r population. (c) Log-log diagrams for grain size distribution (grain number vs. grain diameter) of cataclastic rock samples from the Presenzano fault core. Sample location along PSZ-1 scan-line is in (a).

rocks. Fracturing in damage zones occurs in the early stages of faulting overprinting/reactivating pre-existing foliations in the protolith (e.g. Willemse et al., 1997; Petit et al., 1999; Salvini et al., 1999; Shipton and Cowie, 2001). In particular, a dominant fracture set with closely spaced surfaces forms ahead of the fault tip, its attitude depending on the fault geometry and kinematics (e.g. Petit and Barquins, 1988; Salvini et al., 1999). The intersection at high angles between this fracture set and pre-existing or newly formed foliations (e.g. joints or bedding) produces orthorhombic lithons (Fig. 13a). As faulting evolves, deformation concentrates in preferential sectors of damage zones (Fig. 13b), where additional fracturing reduces the original size of rock lithons (Fig. 14). The shape anisotropy associated with the

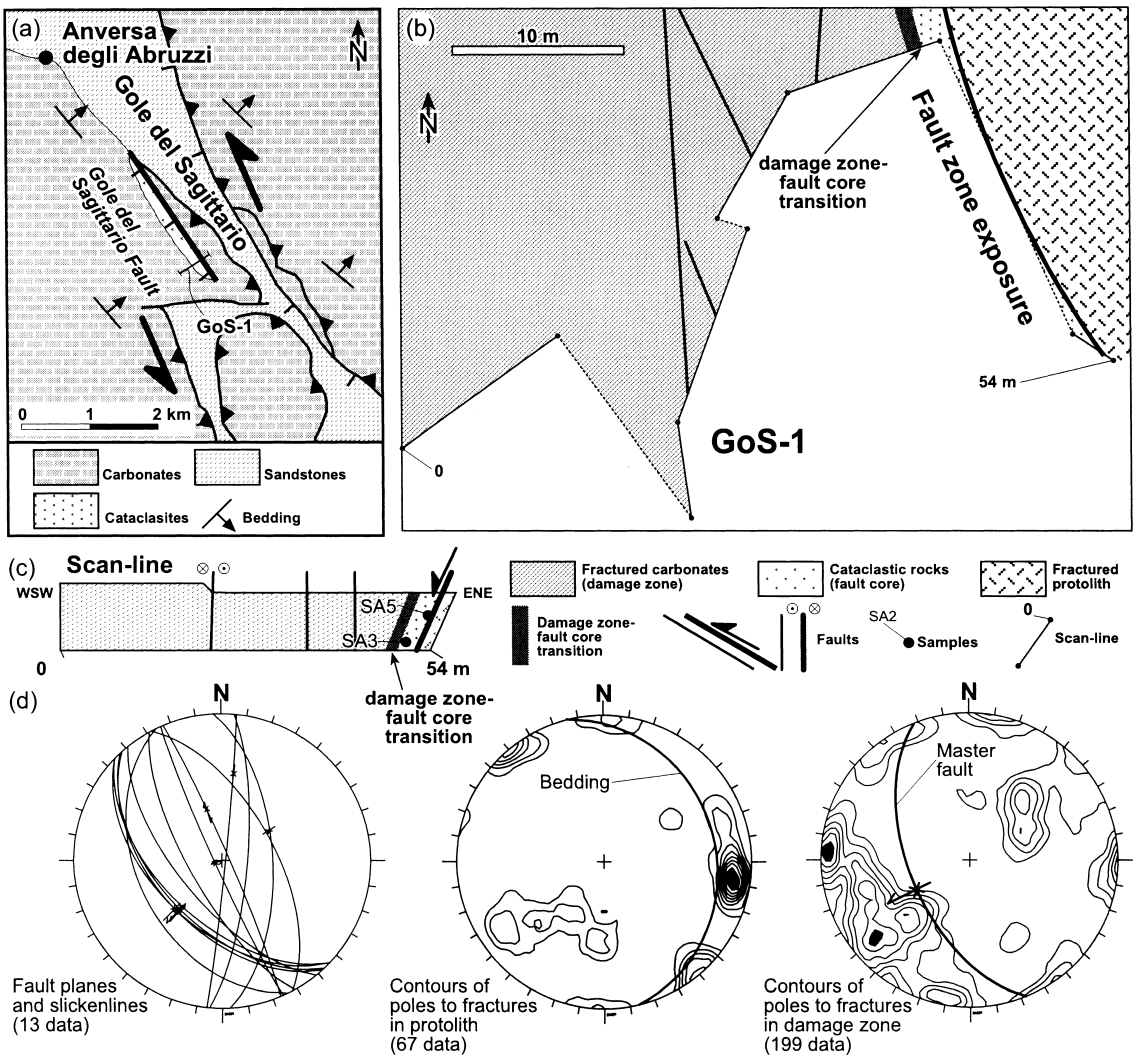

Fig. 10. (a) Structural map for the Gole del Sagittario Fault area. (b) Map view for GoS-1 scan-line across the Gole del Sagittario Fault. (c) Schematic cross-section for GoS-1 scan-line. (d) Stereograms (Schmidt projections, lower hemisphere) of structural data for GoS-1 scan-line.

orthorhombic symmetry of these lithons eases jointing perpendicular to their long symmetry axes (e.g. Engelder, 1987; Ramsay and Lisle, 2000). This process is easily demonstrated by considering the fibre stress (i.e. the stress parallel to the long axis) generated during bending of an elongated plate (i.e. the orthorhombic rock lithons in our example), subject to a concentrated force V_a (Turcotte and Schubert, 1982). In order to apply the linear elastic theory, the plate has to be thin compared with its width ($h \ll L$) and the deflection of the plate, w, has to be small compared with the plate width ($w \ll L$). In such a system, the maximum fibre stress σ_{xx} is given by

$$\sigma_{xx} = -6M/h^2 \tag{2}$$

where M is the applied bending moment that is given by

$$M = -V_a \times L/2 \tag{3}$$

By applying Eqs. (2) and (3) to the orthorhombic carbonate lithons (i.e. lithon thickness = cleavage spacing ≈ 0.01 m; lithon width = layer thickness ≈ 1 m) and overestimating their tensile strength (i.e. $\sigma_{xx} \approx 30 \times 10^6$ Pa; Paterson, 1978) in order to take into account the effect of lithostatic load on the material strength, we obtain the applied force V_a as

$$V_a = \sigma_{xx} \times h^2/3 \approx 1000 \text{ N} \tag{4}$$

that is a value commonly reached within fault zones during faulting (Turcotte and Schubert, 1982).

The long and short symmetry axes switch with each other during lithon fracturing (Fig. 14). Subsequently, the direction of preferential fracturing changes as well, forming at least two fracture sets in addition to the dominant one. Repeated switch of symmetry axes causes the progressive modification of lithon symmetry during their size reduction, such that their shape evolves from orthorhombic to quasi-isometric (Fig. 14c). Owing to the shape anisotropy decrease, the internal strength of rock lithons increases and, eventually, further anisotropy-controlled jointing is

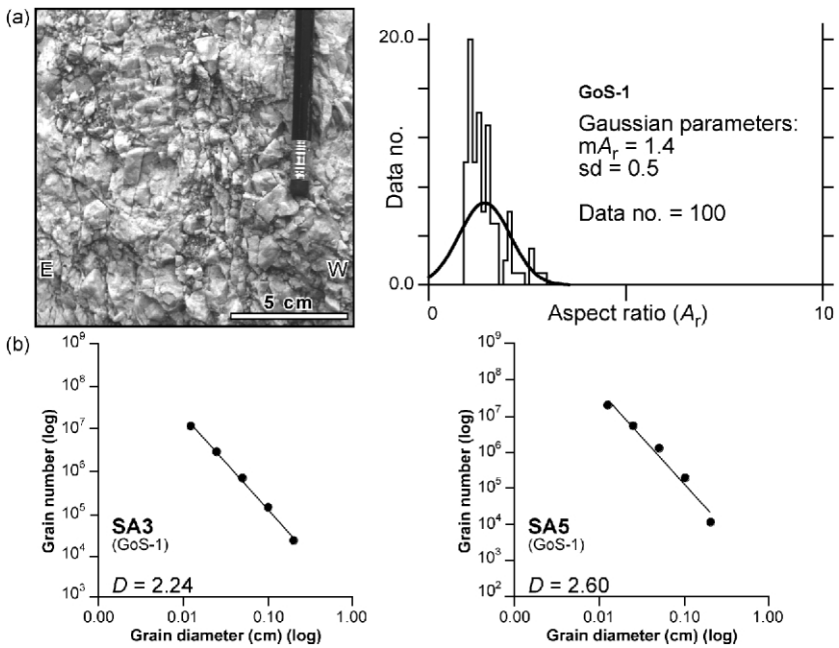

Fig. 11. (a) Outcrop photograph and histogram of A_r (L/l, aspect ratio of lithon sections) at DZ–FC transition for GoS-1 scan-line. Solid line in histogram is the Gaussian curve best fitting A_r population. (b) Log-log diagrams for grain size distribution (grain number vs. grain diameter) of cataclastic rock samples from the Gole del Sagittario fault core. Sample location along GoS-1 scan-line is in Fig. 10c.

inhibited. This roughly isometric symmetry favours rigid-body rotation of rock lithons instead of further jointing. These conditions are initially reached in localised rock masses constituting embryonic fault cores (Fig. 13b), where comminution of rock prisms starts during particle rotation. Eventually, a mature fault core develops from the embryonic fault core. Slip localisation favours development of second-order fault surfaces within the fault core (Fig. 13c).

4.2. Comparison with deformation bands

Our results suggest that, once a granular fabric develops in embryonic carbonate fault cores (Fig. 13b and c), their further evolution should be significantly similar to the development of deformation bands from clastic rocks (Aydin, 1978; Aydin and Johnson, 1978, 1983; Antonellini et al., 1994; Antonellini and Pollard, 1995; Morgan, 1999; Morgan and Boettcher, 1999). Clastic rocks (e.g. sandstone) consist of aggregates of variably cemented, sorted and shaped particles. Deformation bands develop by a combination of processes including cataclasis, grain rotation and mixing of grains and grain fragments with the matrix (Aydin, 1978; Ogilvie and Glover, 2001). The initial stages of deformation band development are characterised by sliding and rigid-body rotation of grains (Antonellini et al., 1994), during which fracturing of the grains is controlled by contact geometry (Gallagher, 1974). The generation of fault cores from poorly layered limestone requires a longer evolution and a higher activation energy due to initial processes such as multiple fracturing and comminution preceding the generation of nearly isometric lithons. When a degree of roundness comparable with that of particles in clastic sediments is reached by lithon grinding and abrasion, further evolution of the cataclastic process in poorly cohesive carbonate fault core rocks is expected to be comparable with the growth of deformation bands. The much lower activation energy for the nucleation of deformation bands in clastic rocks explains their common occurrence in low-displacement faults in sandstones (Aydin, 1978; Davis, 1999). Conversely, fault cores are rarer in low-displacement faults in limestone (e.g. Peacock et al., 1999).

4.3. Comparison with available particle size data

Particle-size data of cataclastic rocks from the studied bulk fault cores are power-law distributed with average fractal dimensions $D \approx 2.5–2.6$. This agrees with previous field (e.g. Sammis et al., 1987) and experimental works (Biegel et al., 1989; Marone and Scholz, 1989) and with numerical models (Morgan, 1999). Such distribution represents a cataclastic fabric, in which the probability of fracturing particles having similar size is reduced to the minimum (Sammis et al., 1987; Marone and Scholz, 1989). According to Storti et al. (2003), 2.6–2.7 is possibly the highest fractal dimension in cataclastic rocks from bulk carbonate fault cores. The cataclastic fabric associated with these fractal dimensions likely enhances slip localisation and the subsequent formation of narrow shear zones where most displacement is accommodated.

4.4. Role of pressure solution

In the studied fault zones, solution cleavages are well

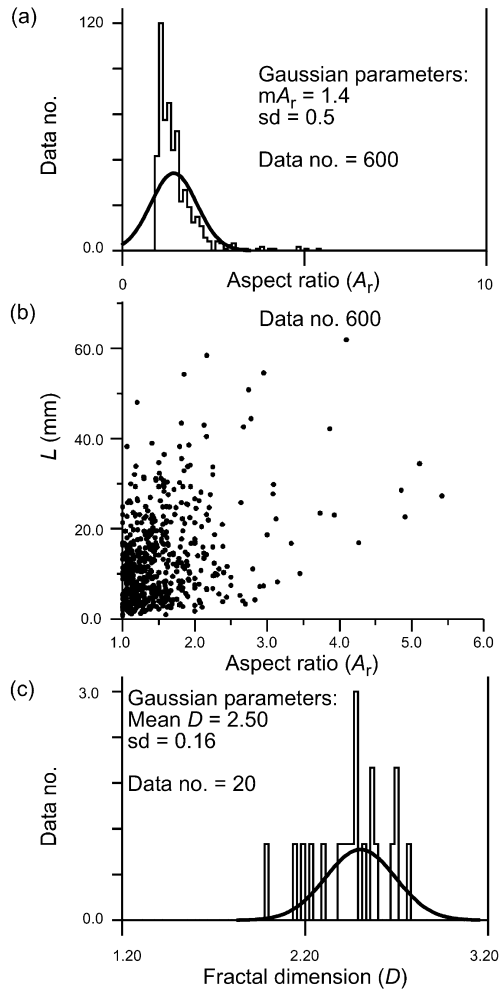

Fig. 12. (a) Histogram of the entire A_r (L/l, aspect ratio of lithon sections at DZ–FC transitions) population in this article. Solid line is the Gaussian curve best fitting A_r population. (b) Diagram of the entire A_r population plotted against L (short side of lithon sections). (c) Histogram of the entire D (fractal dimension from particle size distributions of cataclastic rocks) population in this article. Solid line is the Gaussian curve best fitting D population.

developed in the damage zones (e.g. Billi, 2003) in association with subordered calcite-filled veins. On the contrary, evidence of bulk pressure solution is lacking in the fault cores. It is known that the efficiency of dissolution in limestone is maximised at low strain rates and high fluid flows, in addition to high particle surface to volume ratios and to an appropriate content of clay (Rutter, 1976). This suggests that pressure solution occurred in the early stage of faulting (e.g. Salvini et al., 1999), enhanced by low strain rates and fracture-related efficient fluid circulation. Pressure solution should have been progressively inhibited during fault core development. Possible reasons for this include faster strain rates and decreasing efficiency of fluid circulation owing to particle size reduction (e.g. Antonellini and Aydin, 1994).

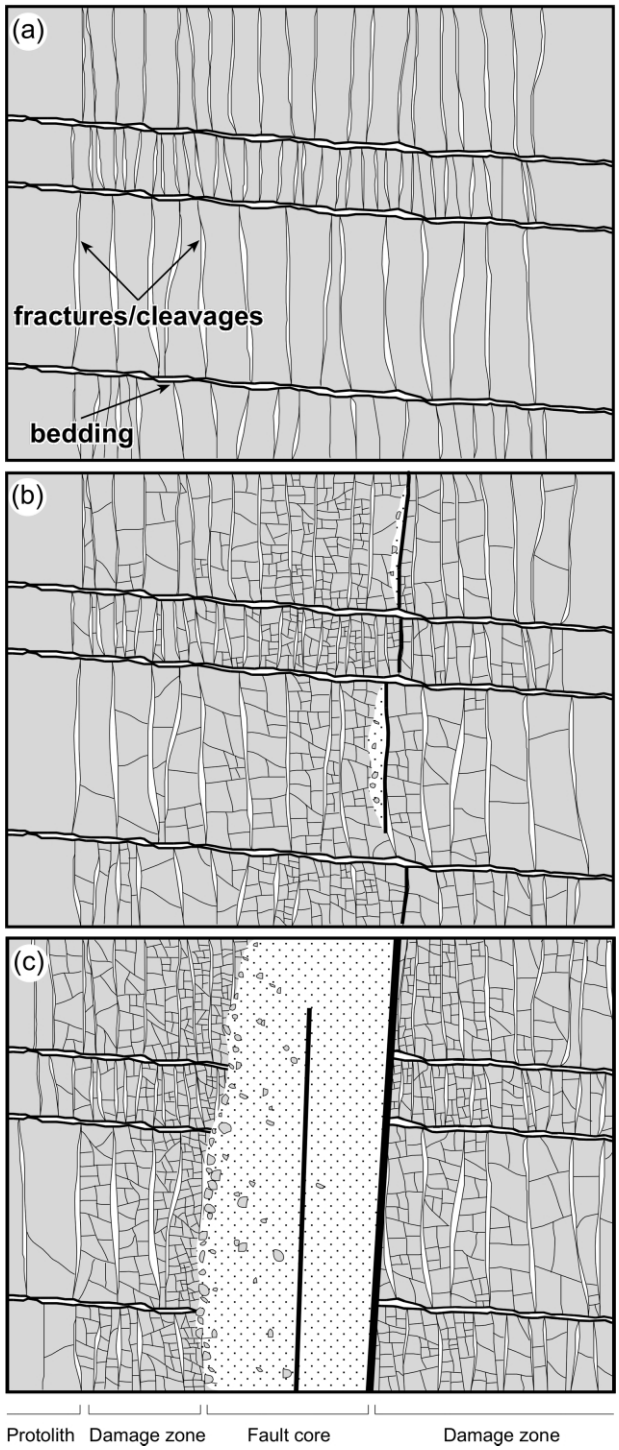

Fig. 13. 2-D evolutionary model for an ideal sub-vertical fault zone (vertical cross-sections). (a) Pre-existing or early-formed fractures/cleavages commonly develop perpendicularly to the bedding attitude. (b) As faulting progresses, damage concentrates and an embryonic fault core develops. (c) As displacement increases, the fault core develops. Cataclastic rocks in fault core are generated from a pristine damage zone, in which a critical rock fabric consisting of nearly isometric lithons developed. Second-order faults can develop within fault core.

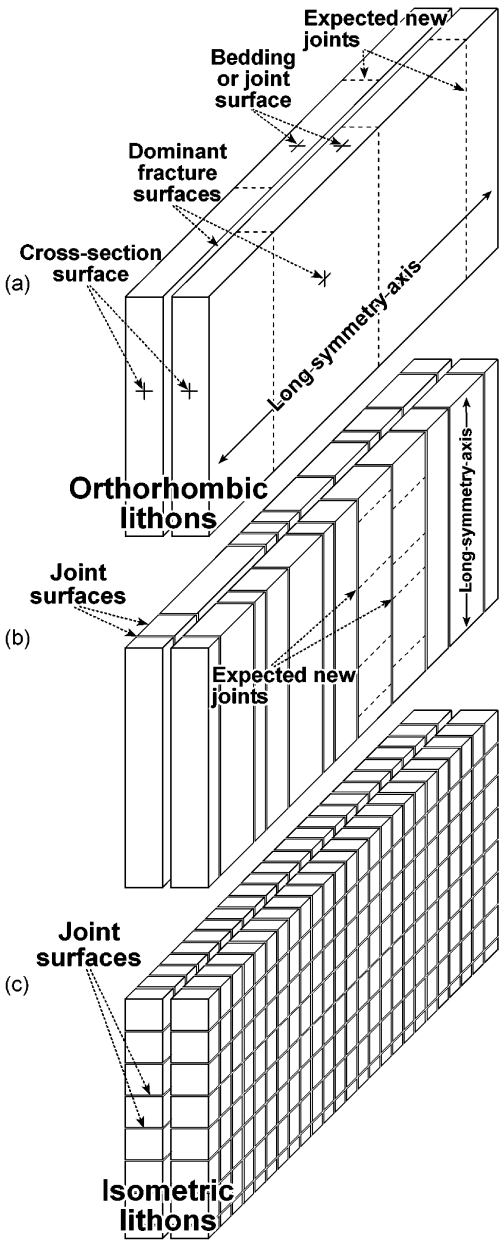

Fig. 14. Conceptual model for anisotropy-controlled progressive fracturing of orthorhombic rock lithons into isometric lithons. The model is simplified in three steps. (a) Orthorhombic lithons are generated by the sub-perpendicular intersection between a dominant fracture set and a subordered one (e.g. joints or bedding). (b) A set of joints dissects orthorhombic lithons perpendicularly to their long axis. Joints are preferentially sub-vertical by the effect of lithostatic overburden. Lithons (nearly tetragonal) with vertical long axis are generated. (c) A second set of joints dissects tetragonal lithons perpendicularly to the long axis and isometric lithons are generated.

4.5. Insights into the spatial and temporal evolution of fault zone permeability

The permeability architecture of a mature fault zone consists of two main components (Fig. 15a and b): the damage zone, which has the highest permeability, and the fault core, which constitutes a low-permeability sector (e.g. Antonellini and Aydin, 1994, 1995; Caine et al., 1996). In our model, this is not a static picture but a complex evolving system in both space and time. Two main stages can be recognised in a two-dimensional description of the fault zone permeability evolution: (1) the conduit stage, which precedes the development of the fault core (Fig. 15a). During this initial stage, the progression of fracturing increases the permeability of the fault zone, which behaves as a self-enhancing conduit for fluid flow. Just before the onset of fault core development, the most evolved sector of the damage zone consists of centimetre-sized quasi-isometric lithons. The foliation network ensures a very efficient connectivity and fluid flow. When particle rotation starts, the permeability structure of the fault zone is disrupted and (2) the evolved stage initiates (Fig. 15b). Particle rotation and comminution increase the fine-grained matrix within the particle population and dramatically reduce fracture connectivity and permeability. The fault core starts to seal and eventually behaves as a barrier against fluid flow. At this stage, fluid flow is localised in the damage zone, particularly near the boundary with the fault core where a remnant of the most highly fractured sector is preserved. Outcrop-scale field evidences in the studied fault zones support the sealing behaviour of fault cores and the leaking one of damage zones (Fig. 15c).

The permeability evolution of propagating fault zones is a four-dimensional process. Different permeability properties occur in different regions of the fault zone at different evolutionary stages. Ahead of the fault tip, the fault zone is in an embryonic stage (only damage zone) and rocks behave as a preferential conduit for fluid flow (i.e. conduit stage). The lateral propagation of the fault core dissects the across and along strike continuity of the conduit and causes its compartmentalisation into sectors with low hydraulic exchanges (Fig. 15d).

5. Conclusions

We studied DZ–FC transitions in fault zones developed from shallow-water carbonate protoliths. Despite different sizes, kinematics, and inherited structural fabrics of the protoliths, rocks in damage zones adjacent to fault cores show very similar structural fabrics, which consist of tightly juxtaposed and interlocked, nearly isometric lithons a few centimetres in size, having a cross-sectional aspect ratio of about 1.4. We interpret this value as the shape upper limit for the systematic initiation of particle rotation and grinding, which enhance the formation of fault core rocks by cataclastic flow.

Our structural observations at the DZ–FC transition and the particle-size distribution of bulk fault core rocks in the studied fault zones support a two-stage evolutionary model. The first stage is dominated by fracturing during the evolution of the damage zone, which provides a high permeability conduit for fluid flow. The second stage

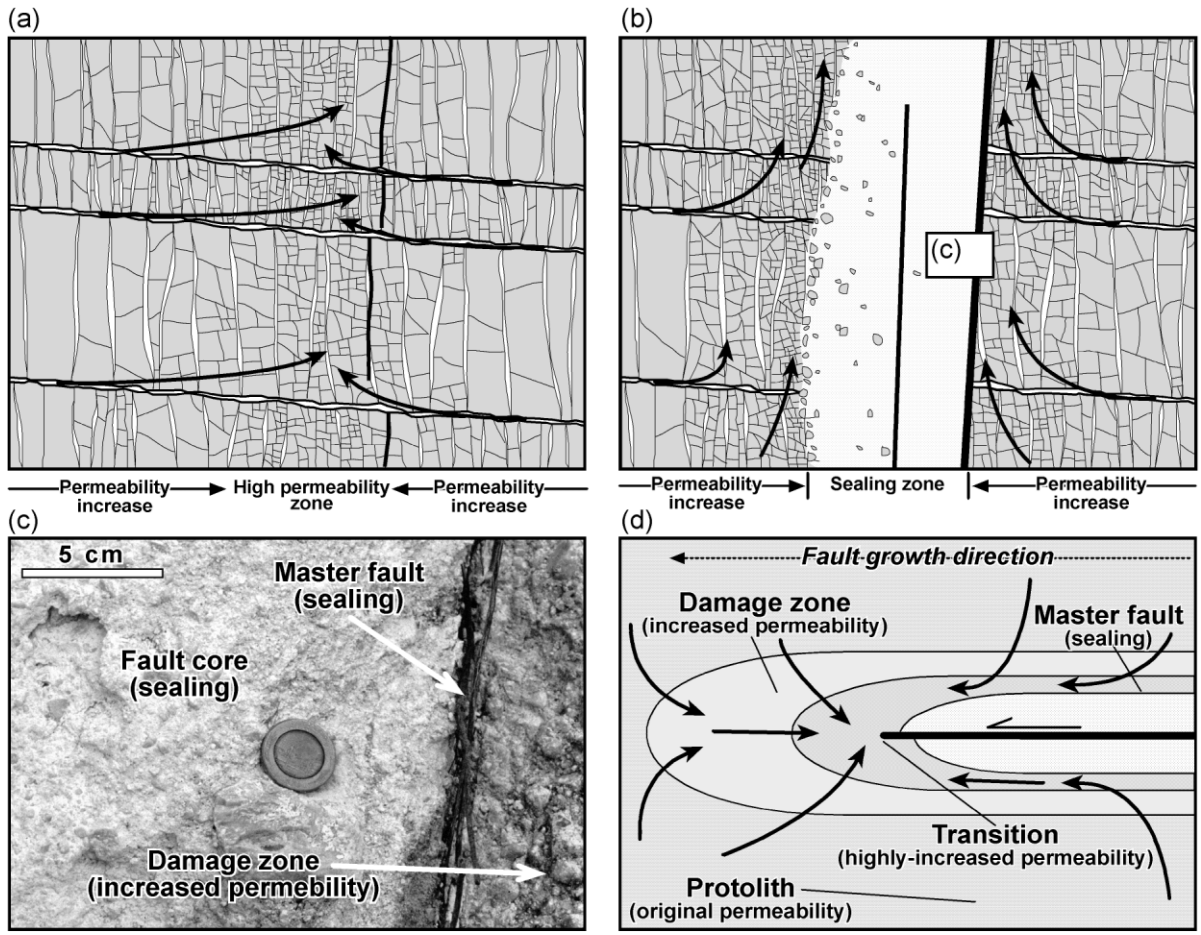

Fig. 15. Permeability and fluid circulation model. Black arrows are possible fluid flow trajectories. (a) Model for permeability compartmentalisation in a growing fault zone with a developed damage zone and an embryonic fault core (cross-section). (b) Model for permeability compartmentalisation in a mature fault zone with developed damage zone and fault core (cross-section). (c) Outcrop photograph (vertical cross-section) from the Mattinata Fault zone. Note that the damage zone (on the right) is impregnated by iron hydroxides (darker material), whereas the fault core is not impregnated, attesting to its lower permeability. (d) Conceptual model of a growing fault zone and permeability compartmentalisation.

includes the development of the fault core, which occurs in the most fractured region of the damage zone by rotation and comminution of rock particles once they reach a nearly isometric shape. Such an evolutionary pathway, when applied to the four-dimensional evolution of fault zones, gives complex permeability patterns that have important implications for fluid migration through faulted rock bodies.

Acknowledgements

Part of the analysed data derives from a study on cataclasis in carbonate rocks supported by Enterprise Oil Ltd. We wish to thank R. Gambini for his encouragement and advice, S. Laubach and A. Younes for a critical reading of an earlier version of the manuscript, and J. Evans, J. Hadizadeh and P. Labaume for providing insightful reviews. P. Impagliazzo, S. Merlo and M. Musacchio helped in data collection and analysis during field and laboratory work.

References

Allègre, C.J., Le Mouel, J.L., Provost, A., 1982. Scaling rules in rock fracture and possible implications for earthquake predictions. Nature 297, 47–49.

Antonellini, M., Aydin, A., 1994. Effect of faulting on fluid flow in porous sandstones: petrophysical properties. American Association of Petroleum Geologists Bulletin 78, 355–377.

Antonellini, M., Aydin, A., 1995. Effect of faulting on fluid flow in porous sandstones: geometry and spatial distribution. American Association of Petroleum Geologists Bulletin 79, 642–671.

Antonellini, M., Pollard, D.D., 1995. Distinct element modeling of deformation bands in sandstones. Journal of Structural Geology 17, 1165–1182.

Antonellini, M., Aydin, A., Pollard, D.D., 1994. Microstructure of deformation bands in porous sandstones at Arches National Park, Utah. Journal of Structural Geology 16, 941–959.

Aydin, A., 1978. Small faults formed as deformation bands in sandstone. Pure and Applied Geophysics 116, 913–930.

Aydin, A., Johnson, A.M., 1978. Development of faults as zones of deformation bands and as slip surfaces in sandstone. Pure and Applied Geophysics 116, 931–942.

Aydin, A., Johnson, A.M., 1983. Analysis of faulting in porous sandstones. Journal of Structural Geology 5, 19–31.

Biegel, R.L., Sammis, C.G., Dieterich, J.H., 1989. The frictional properties of a simulated gouge having a fractal particle distribution. Journal of Structural Geology 11, 827–846.

Billi, A., 2003. Solution slip and separations on strike-slip fault zones: theory and application to the Mattinata Fault, Italy. Journal of Structural Geology 25, 703–715.

Billi, A., Salvini, F., 2000. Sistemi di fratture associati a faglie in rocce carbonatiche: nuovi dati sull'evoluzione tettonica del Promontorio del Gargano. Bollettino della Società Geologica Italiana 119, 237–250.

Billi, A., Salvini, F., 2001. Characterisation of fracture patterns in exposed carbonate reservoirs of the Southern Apennines, Italy. Journal of Petroleum Geology 24, 147–169.

Billi, A., Storti, F., Salvini, F., 2003. Particle size distributions of fault rocks and fault transpression: are they related? Terra Nova 15, 61–66.

Blenkinsop, T.G., 1991. Cataclasis and processes of particle-size reduction. Pure and Applied Geophysics 136, 59–86.

Bosi, V., Giordano, G., 1997. Stress field evolution in central Italy during middle-late Pleistocene: new information from southern Latium. Il Quaternario 10, 631–636.

Caine, J.S., Evans, J.P., Forster, C.B., 1996. Fault zone architecture and permeability structure. Geology 24, 1025–1028.

Chester, F.M., Evans, J.P., Biegel, R.L., 1993. Internal structure and weakening mechanisms of the San Andreas Fault. Journal of Geophysical Research 98, 771–786.

Cladouhos, T.T., Marrett, R., 1996. Are fault growth and linkage models consistent with power-law distributions of fault lengths? Journal of Structural Geology 18, 281–293.

Davis, G.H., 1999. Structural geology of the Colorado Plateau region of southern Utah, with special emphasis on deformation bands. Geological Society of America Special Papers 342.

Davis, G.H., Reynolds, S.J., 1996. Structural Geology of Rocks and Regions, Wiley, New York.

Engelder, J.T., 1974. Cataclasis and the generation of fault gouge. Geological Society of America Bulletin 85, 1515–1522.

Engelder, J.T., 1987. Joints and shear fractures in rock. In: Atkinson, B.K., (Ed.), Fracture Mechanics of Rock, Academic Press, London, pp. 27–69.

Evans, J.P., 1990. Textures and deformation mechanisms and the role of fluids in cataclastically deformed granitic rocks. In: Knipe, R.J., Rutter, E.H. (Eds.), Deformation Mechanisms, Rheology, and Tectonics. Geological Society Special Publication 54, pp. 29–39.

Evans, J.P., Langrock, H., 1994. Structural analysis of the Brigham City–Weber Segment Boundary zone, Wasatch normal fault zone, Utah: implications for fault growth and structure. Pure and Applied Geophysics 142, 663–685.

Evans, J.P., Forster, C.B., Goddard, J.V., 1997. Permeabilities of fault-related rocks and implications for fault-zone hydraulic structure. Journal of Structural Geology 19, 1393–1404.

Gallagher, J.J., 1974. Experimental studies relating to microfracture in sandstone. Tectonophysics 21, 243–247.

Hadizadeh, J., Rutter, E.H., 1983. The low temperature brittle-ductile transition in quartzite and occurrence of cataclastic flow in nature. Geologische Rundschau 72, 493–503.

Hesthammer, J., Johansen, T.E.S., Watts, L., 2000. Spatial relationships within fault damage zones in sandstone. Marine and Petroleum Geology 17, 873–893.

Knipe, R.J., 1997. Juxtaposition and seal diagrams to help analyze fault seals in hydrocarbon reservoirs. American Association of Petroleum Geologists Bulletin 81, 187–195.

Mandl, G., de Jong, L.N.J., Maltha, A., 1977. Shear zones in granular material: an experimental study of their structure and mechanical genesis. Rock Mechanics 9, 95–144.

Manzocchi, T., Walsh, J.J., Nell, P., Yielding, G., 1999. Fault transmissibility multipliers for flow simulation models. Petroleum Geoscience 5, 53–63.

Marone, C., 1995. Fault zone strength and failure criteria. Geophysical Research Letters 22, 723–726.

Marone, C., Scholz, C.H., 1989. Particle-size distribution and microstructures within simulated fault gouge. Journal of Structural Geology 11, 799–814.

McGrath, A.G., Davison, I., 1995. Damage zones geometry around fault tips. Journal of Structural Geology 17, 1011–1024.

Miccadei, E., 1993. Geologia dell'area Alto Sagittario-Alto Sangro (Abruzzo, Appennino Centrale). Geologica Romana 29, 463–481.

Morgan, K.J., 1999. Numerical simulations of granular shear zones using the distinct element method. 2. Effects of particle-size distribution and interparticle friction on mechanical behavior. Journal of Geophysical Research 104, 2721–2732.

Morgan, K.J., Boettcher, M.S., 1999. Numerical simulations of granular shear zones using the distinct element method. 1. Shear zone kinematics and the micromechanics of localization. Journal of Geophysical Research 104, 2703–2719.

Newman, J., Mitra, G., 1993. Lateral variations in mylonite zone thickness as influenced by fluid-rock interactions, Linville Falls Fault, North Carolina. Journal of Structural Geology 15, 849–863.

Ogilvie, S.R., Glover, P.W.J., 2001. The petrophysical properties of deformation bands in relation to their microstructure. Earth and Planetary Science Letters 193, 129–142.

Parotto, M., 1971. Stratigraphy and tectonics of eastern Simbruini and western Marsica ranges (central Apennines—Italy). Memorie dell'Accademia Nazionale dei Lincei (sezione II) 10, 9–170.

Parotto, M., Praturlon, A., 1975. Geological summary of the central Apennines. In: Ogniben, L., Parotto, M., Praturlon, A. (Eds.), Structural Model of Italy. Quaderni della Ricerca Scientifica del Comitato Nazionale per le Ricerche 90, pp. 257–311.

Paterson, M.S., 1978. Experimental Rock Deformation—The Brittle Field, Springer Verlag, Berlin.

Peacock, D.C.P., Fisher, Q.J., Willemse, E.M.J., Aydin, A., 1999. The relationship between faults and pressure solution seams in carbonate rocks and the implications for fluid flow. In: Jones, G., Fisher, Q.J., Knipe, R.J. (Eds.), Faulting, Fault Sealing and Fluid flow in Hydrocarbon Reservoirs. Geological Society Special Publication 147, pp. 105–115.

Petit, J.-P., Barquins, M., 1988. Can natural faults propagate under mode-II conditions? Tectonics 7, 1243–1256.

Petit, J.-P., Wibberley, C.A.J., Ruiz, G., 1999. 'Crack-seal' slip: a new fault valve mechanism? Journal of Structural Geology 21, 1199–1207.

Pollard, D.D., Aydin, A., 1988. Progress in understanding jointing over the past century. Geological Society of America Bulletin 100, 1181–1204.

Ramsay, J.G., Lisle, R.J., 2000. The Techniques of Modern Structural Geology, Academic Press, London.

Rutter, E.H., 1976. The kinetics of rock deformation by pressure solution. Philosophical Transactions of Royal Society of London 283, 203–219.

Salvini, F., Billi, A., Wise, D.U., 1999. Strike-slip fault-propagation cleavage in carbonate rocks: the Mattinata Fault zone. Journal of Structural Geology 21, 1731–1749.

Sammis, C.G., Biegel, R., 1989. Fractals, fault gouge, and friction. Pure and Applied Geophysics 131, 256–271.

Sammis, C.G., Osborne, R.H., Anderson, J.L., Banerdt, M., White, P., 1986. Self-similar cataclasis in the formation of fault gouge. Pure and Applied Geophysics 124, 53–78.

Sammis, C.G., King, G., Biegel, R., 1987. The kinematics of gouge deformation. Pure and Applied Geophysics 125, 777–812.

Schulz, S.E., Evans, J.P., 1998. Spatial variability in microscopic deformation and composition of the Punchbowl fault, Southern California: implications for mechanisms, fluid-rock interaction, and fault morphology. Tectonophysics 295, 223–244.

Schulz, S.E., Evans, J.P., 2000. Mesoscopic structure of the Punchbowl Fault, Southern California and the geological and geophysical structure of active strike-slip fault. Journal of Structural Geology 22, 913–930.

Shipton, Z.K., Cowie, P.A., 2001. Damage zone and slip-surface evolution over mm to km scales in high-porosity Navajo sandstone, Utah. Journal of Structural Geology 23, 1825–1844.

Sibson, R.H., 1977. Fault rock and fault mechanisms. Journal of the Geological Society 133, 191–213.

Storti, F., Billi, A., Salvini, F., 2003. Particle size distributions in natural carbonate fault rocks: insights for non-self-similar cataclasis. Earth and Planetary Science Letters 206, 173–186.

Turcotte, D.L., 1986. Fractals and fragmentation. Journal of Geophysical Research 91, 1921–1928.

Turcotte, D.L., Schubert, G., 1982. Geodynamics. Applications of Continuum Physics to Geological Problems, John Wiley and Sons, New York.

Willemse, E.J.M., Peacock, D.C.P., Aydin, A., 1997. Nucleation and growth of strike-slip faults in limestones from Somerset, UK. Journal of Structural Geology 19, 1461–1477.

Yielding, G., Øverland, J.A., Byeberg, G., 1999. Characterization of fault zones for reservoir modeling: an example from the Gullfaks Field, Northern North Sea. American Association of Petroleum Geologists Bulletin 83, 925–951.